Slit Beam Shaping for Femtosecond Laser Point-by-Point Inscription of High-Quality Fiber Bragg Gratings

Xizhen Xu, Jun He, *Member, OSA*, Jia He, Baijie Xu, Runxiao Chen, Kaiming Yang, Changrui Liao, Yatao Yang, and Yiping Wang, *Senior Member, IEEE, Senior Member, OSA*

***Abstract*—Fiber Bragg gratings (FBGs) inscribed by using femtosecond laser point-by-point (PbP) technology typically have high birefringence due to the elliptical cross-sectional pattern of refractive index modulations (RIMs) created in the fiber core. Additionally, a highly reflective type II PbP FBG, which has a large coupling coefficient, also exhibits large insertion loss due to the limited RIM area induced by a single femtosecond laser pulse. Here we demonstrate a slit beam shaping method for femtosecond laser PbP inscription of high-quality FBGs, featuring by high reflectivity, low insertion loss, and low birefringence. The slit beam shaping method could reduce the ellipticity in the cross-sectional pattern of RIMs without reducing the cross-sectional area, leading to low birefringence and low insertion loss. The experimental results agree well with numerical calculations. Hence, a high-quality type II PbP FBG, which has high reflectivity of 99.12% (i.e., Bragg resonance attenuation of 20.52 dB), low insertion loss of 0.30 dB, and low birefringence of 1.86×10^{-6}, was successfully created by use of a slit width of 0.8 mm. Moreover, an enlarged cross-sectional area was created by use of a slit width of 0.2 mm, resulting in a high ratio of 172.46 of the coupling strength coefficient to the scattering loss coefficient in the fabricated PbP FBG, which exhibits very high reflectivity of 99.99% (i.e., a strong Bragg resonance attenuation of 46.65 dB) and low insertion loss of 0.27 dB. Such high-quality FBGs will be promising in many applications, such as optical fiber communications, sensors, and lasers.**

***Index Terms*—Fiber Bragg gratings, laser materials processing, slit beam shaping.**

I. Introduction

HIGH-QUALITY fiber Bragg gratings (FBGs) with high reflectivity, low insertion loss, and low birefringence have received much attention in many areas, such as fiber-optic communications, sensors and lasers. The insertion loss (IL), as one of the key parameters of FBGs, can restrict the multiplexing capability of FBG sensors arrays and the efficiency of fiber lasers [1], [2]. The polarization dependent loss (PDL), resulting from the laser-induced birefringence in FBGs, will deteriorate the bit error rate in optical transmission systems [3]. To date, various methods have been proposed for fabricating high-quality FBGs. For example, the most commonly used method is the inscription of FBGs by femtosecond laser exposure through a phase mask [4], [5]. However, it is difficult to use this method for creating a wavelength-division-multiplexed FBG array. Additionally, the femtosecond laser point-by-point (PbP) or line-by-line (LbL) inscription method was used to create FBGs with various Bragg wavelengths [1], [2], [6]–[9]. In comparison with the LbL inscription method, the PbP inscription method has a similar flexibility but a much higher efficiency in grating fabrication, and hence attracted much interest in recent years [1], [10]–[12]. Nevertheless, the cross-sectional pattern of refractive index modulations (RIMs) induced by a single femtosecond laser pulse is elliptical, resulting in high birefringence [2], [9]. Moreover, the RIM area is limited, resulting in a low ratio of the coupling strength coefficient to the scattering loss coefficient κ/α (i.e., < 100) [13], [14]. In our previous work, we demonstrated a method for reducing the PDL (as low as 1.18 dB) and increasing the κ/α of PbP FBGs based on a symmetric cross-sectional pattern of RIMs formed in parallel-integrated FBGs [12]. However, it is complicated and also inefficient for fabricating these special spatial-distributed parallel-integrated FBGs.

Spatial beam shaping method has been developed for creating PbP FBGs by use of femtosecond laser inscription [14]–[16]. Various optical setups, such as two cylindrical lenses [17], a spatial light modulator (SLM) [18], [19] and a slit [20], are used for spatial beam shaping. Recently, the slit beam shaping method was proposed to create near-circular cross-sectional patterns of PbP FBG [16]. However, the quality of the fabricated FBG

Manuscript received January 29, 2021; revised April 8, 2021 and May 17, 2021; accepted May 18, 2021. Date of publication May 21, 2021; date of current version August 2, 2021. This work was supported in part by the National Natural Science Foundation of China under Grants U1913212, 61875128, and 62005170, in part by Department of Science and Technology of Guangdong Province under Grants 2019TQ05X113, 2019A1515111114, and 2019A1515011393, in part by Shenzhen Science and Technology Program under Grants RCYX20200714114538160, JCYJ20200109114201731, and JCYJ20180507182058432, and in part by China Postdoctoral Science Foundation under Grant 2019M663049. *(Corresponding author: Jun He).*

Xizhen Xu, Jun He, Jia He, Baijie Xu, Runxiao Chen, Kaiming Yang, Changrui Liao, and Yiping Wang are with the Key Laboratory of Optoelectronic Devices and Systems of Ministry of Education/Guangdong Province, College of Physics and Optoelectronic Engineering, Shenzhen University, Shenzhen 518060, China, and also with the Shenzhen Key Laboratory of Photonic Devices and Sensing Systems for Internet of Things, Guangdong and Hong Kong Joint Research Centre for Optical Fibre Sensors, Shenzhen University, Shenzhen 518060, China (e-mail: xizhenxu@szu.edu.cn; hejun07@szu.edu.cn; hejia2019@email.szu.edu.cn; 1900453046@email.szu.edu.cn; 2060453041@email.szu.edu.cn; yangkaiming@email.szu.edu.cn; cliao@szu.edu.cn; ypwang@szu.edu.cn).

Yatao Yang is with the College of Electronics and Information Engineering, Shenzhen University, Shenzhen 518060, China (e-mail: yatao86@163.com).

Color versions of one or more figures in this article are available at https://doi.org/10.1109/JLT.2021.3082566.

Digital Object Identifier 10.1109/JLT.2021.3082566

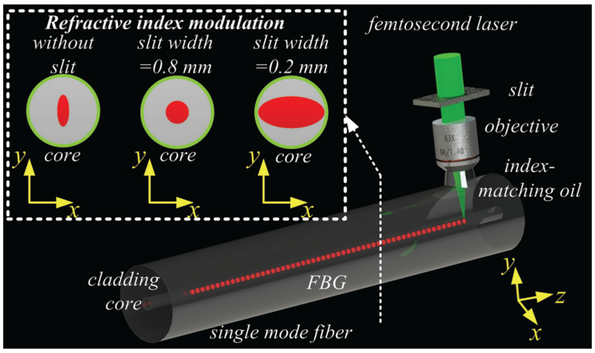

Fig. 1. Schematics of the working principle and experimental setup for fabricating high-quality FBGs using femtosecond laser PbP technology and slit beam shaping method. (Insert: the cross-sectional view of the refractive index modulation created by use of various slit widths.)

mentioned in this paper is quite low, exhibiting low reflectivity of ~60% (i.e., Bragg resonance attenuation of ~4 dB).

In this letter, we further developed the slit beam shaping method for femtosecond laser PbP inscription of high-quality FBGs. The slit beam shaping method reduces the ellipticity in the cross-sectional pattern of RIMs without decreasing the laser beam focus, and leads to low birefringence together with low insertion loss. As a result, a high-quality FBG, which has high reflectivity of 20.56 dB, low insertion loss of 0.30 dB, and low birefringence of 1.86×10^{-6}, was successfully fabricated by using this method with a slit width of 0.8 mm. Moreover, an enlarged cross-sectional area of RIMs could be created by a slit width of 0.2 mm, resulting in a high κ/α of 172.46 in the fabricated PbP FBG.

II. Setup of Fabricating FBG By Using Slit Beam Shaping

The principle and experimental setup used for fabricating high-quality FBGs by using slit beam shaping method and femtosecond laser PbP technology were exhibited in Fig. 1. A frequency-doubled regenerative amplified Yb:KGW ($KGd(WO_3)$) femtosecond laser (Pharos, Light-conversion) with a central wavelength of 514 nm, a pulse width of 290 fs, a repetition rate of 200 kHz, and a laser spot diameter of 3 mm was employed. The repetition rate was lowered to 1 kHz using a pulse picker. Then, an adjustable mechanical slit (Thorlabs, VA100) was inserted in front of the objective. The slit position and inclination was set to ensure the normal incidence of beam center, and the slit orientation was set to parallel to the fiber axis. Subsequently, the laser beam was focused into a single mode fiber (SMF, Corning SMF-28e) by use of a 100× Leica oil-immersion objective with a numerical aperture of 1.25. The output face of the objective and the SMF were immersed in the index matching oil to reduce the aberration at silica/air interfaces. The SMF was moved at a constant velocity using an assembled 3D translation stage (Aerotech ABL15010, ANT130LZS, and ANT130V-5). Consequently, an FBG (i.e., a serial of periodic RIMs) was created in the fiber core along the fiber axis by femtosecond laser pulses. As shown in the inset of Fig. 1, a near-circular cross-sectional pattern of the laser-induced RIM can be obtained after slit beam shaping. The ellipticity in the cross-sectional pattern of RIM can be reduced by carefully adjusting the slit width. Moreover, the enlarged area of cross-sectional pattern of RIM can be obtained by using an appropriate slit width.

TABLE I
Parameter Comparison of Five FBGs (S1-S5)

FBG	W/ mm	*E*/ nJ	*h*/ μm	*w*/ μm	β	*A*/ μm^2	Δn_B	PDL
S1	/	35	3.02	0.86	2.51	2.04	7.57×10^{-5}	12.85
S2	2	32	2.80	1.10	1.54	2.42	5.40×10^{-5}	11.44
S3	1	31	1.84	1.51	0.22	2.18	1.30×10^{-5}	3.48
S4	0.8	30	1.64	1.76	0.07	2.27	1.86×10^{-6}	1.50
S5	0.5	39	1.40	2.54	0.81	2.79	3.60×10^{-5}	9.06

III. Results and Discussion

A. Inscription of FBG With Low Birefringence

At first, we investigated the slit beam shaping method to reduce the laser-induced birefringence in the PbP FBGs. A FBG (i.e., S1) was inscribed by using femtosecond laser PbP technology merely. And four FBGs (i.e., S2, S3, S4, and S5) were inscribed by using femtosecond laser PbP technology and slit beam shaping with a decreasing slit width W shown in Table I. Note that five FBGs, i.e., one FBG S1 inscribed without slit beam shaping and four FBGs S2-S5 inscribed with slit beam shaping, have the same grating pitch of 1.070 μm and the same grating length of 4 mm, and are fabricated by using the same objective. To observe the FBG cross section, we cleaved the FBG at the grating region via a fiber-processing system, consisting of a fiber cleaver (Sumitomo, FC-6S), a microscope (Sunway), and a fiber visual fault locator. The grating region of an FBG could be found by using the visual fault locator, since the red light is scattered out of the fiber core at the FBG position, and then the grating region was held by fiber cleaver. The FBGs S1-S5 were cleaved transversally, and then a microscope (Leica, DM2700MH) with an oil-immersion objective (Leica, 100×, numerical aperture: 1.32) were employed to obtain the cross-sectional images of FBGs. Figs. 2(a1)–(a5) exhibit the cross-sectional microscope images of the five fabricated FBGs S1-S5, respectively, and Figs. 2(b1)–(b5) exhibit the corresponding polarization-resolved transmission spectra and PDL spectra. Note that Figs. 2(b1)–(b5) were directly measured by a Muller-matrix-based commercial polarization analysis system, which consists of a tunable laser (Agilent, 81940A), a polarization synthesizer (Agilent, N7786B), and an optical power meter (Agilent, N7744A). The Bragg wavelengths of these FBGs were determined by applying Gaussian fits on the grating transmission spectra. The five FBGs S1-S5 have similar dip attenuation of -20 dB, and the on-target single pulse energy *E* used for fabricating S1-S5 was shown in Table I. All of them are type II gratings.

Moreover, as shown in Figs. 2(a1)–(a5), the cross-sectional patterns of RIMs are elliptical with various heights *h* and widths *w*. The ellipticity β and area *A* of the cross-sectional patterns of RIMs can be roughly calculated by $\beta = h/w\text{-}1$ and $A = \pi(h \times w)/4$, respectively. In addition, the parameters of cross-sectional patterns of RIMs in FBGs S1-S5 were shown in Table I.

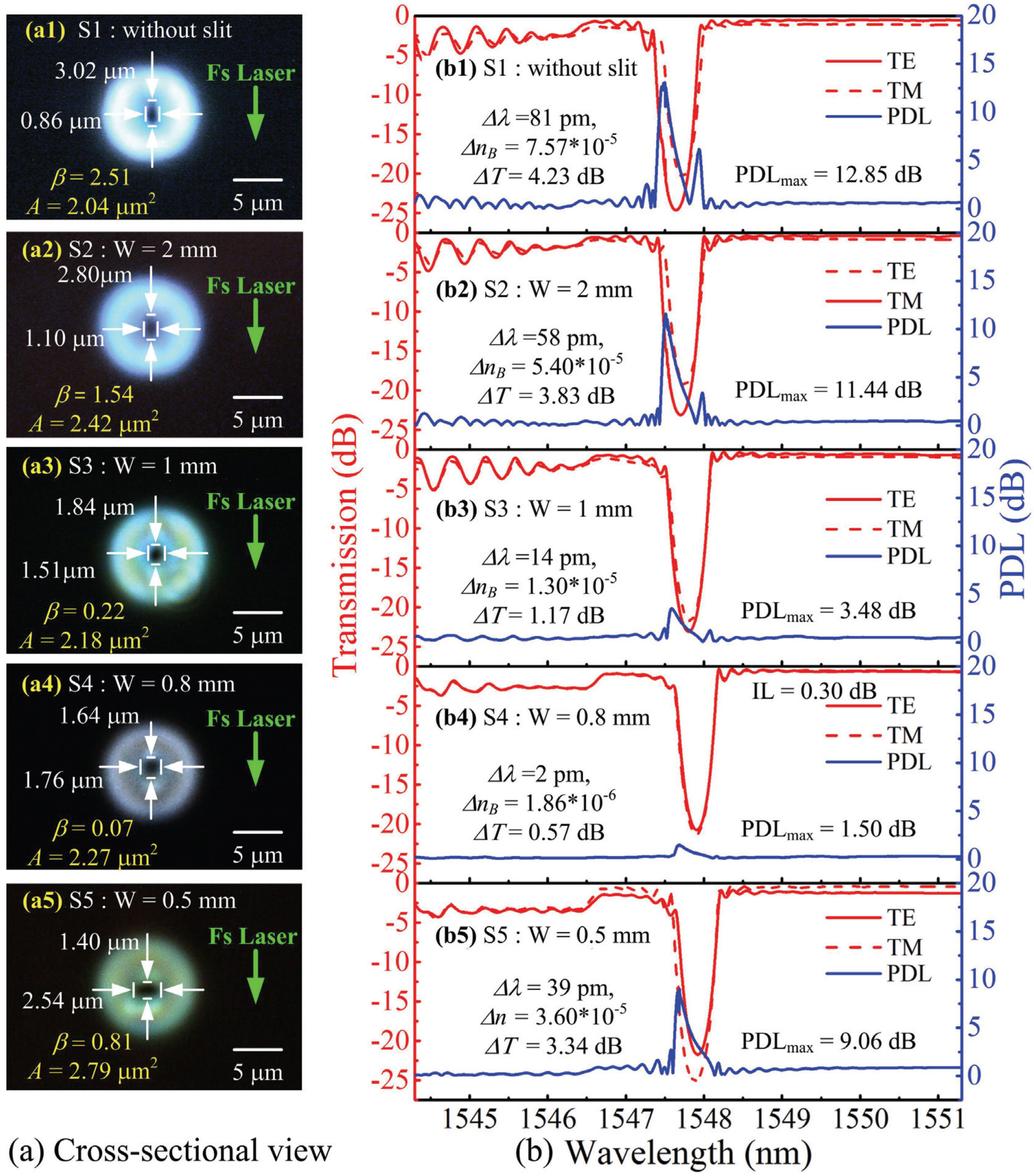

Fig. 2. An FBG S1 inscribed without slit beam shaping and four FBGs S2-S5 inscribed using slit beam shaping with a decreasing slit width (W) of 2, 1, 0.8, and 0.5 mm, respectively. (a) Cross-sectional-view microscope images and (b) corresponding transmission spectra of two orthogonal linear polarization modes (TE and TM), and PDL spectra of FBGs S1-S5.

In case the slit beam shaping is used and the slit width W is reduced, the height of RIM h decreases and the width of RIM w increases, leading to a decrease in the ellipticity of RIM β. For example, as shown in Fig. 2(a1), the FBG S1 inscribed without slit beam shaping has a large ellipticity of 2.51, whereas as shown in Fig. 2(a4), the FBG S4 inscribed with a slit width of 0.8 mm has a minimized ellipticity of 0.07, and the RIM exhibits a near-circular cross-sectional pattern. Additionally, the ellipticity increases again when the slit width W is further reduced to 0.5 mm. Hence, the ellipticity in the cross-sectional pattern of RIM can be reduced to the minimum by using a slit with an appropriate width.

The birefringence in FBGs can be calculated from $\Delta n_B = \Delta\lambda/\Lambda$, where Λ is the grating pitch, $\Delta\lambda$ is the Bragg wavelength difference between two orthogonal linear polarization modes (i.e., TE and TM) [2]. Moreover, ΔT in Fig. 2(b) is the difference in transmission dip attenuation between TE and TM modes. The parameters of the transmission spectra and PDL spectra of FBGs S1-S5 were shown in Table I and Fig. 2(b). Note that FBG S4 fabricated with a slit width of 0.8 mm exhibits a reduced birefringence Δn_B of 1.86×10^{-6} and a reduced PDL of 1.50 dB. It means the birefringence can be reduced effectively by use of the slit beam shaping method via decreasing the ellipticity in the cross-sectional pattern of RIMs.

B. Simulation of Birefringence Effects From RIMs in FBG

Furthermore, we studied the influence of ellipticity in the cross-sectional pattern of RIMs on the birefringence in a PbP FBG by use of a commercial finite element analysis tool

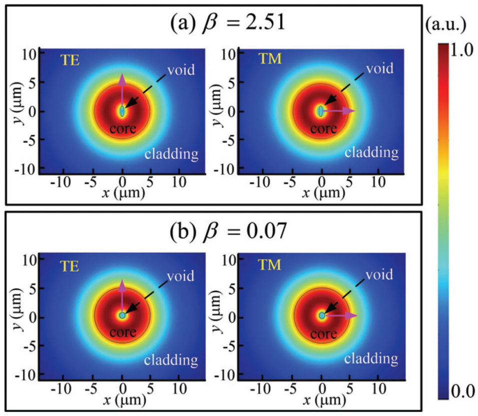

Fig. 3. The simulation of energy flux profiles of two orthogonal linear polarization modes (TE and TM) propagating in the FBGs formed by (a) a series of microvoids with an ellipticity of 2.51 and an area of 0.60 μm^2 and (b) a series of microvoids with a minimized ellipticity of 0.07 and the same area of 0.60 μm^2.

(COMSOL). The RIM model consists of a small microvoid and a surrounded densified region, which was created in the fiber core by high-energy laser-induced micro-explosion. The height and width of the microvoid can be estimated as one half of the densified region [21]. Moreover, the index change in the microvoid is at least one order of magnitude larger than that in the densified region. As a result, the densified region was neglected in the modeling to simplify the calculations. The SMF-28e parameters, i.e., a core diameter of 8.3 μm, a refractive index of 1.44940 and 1.44421 at the wavelength of 1550 nm in fiber core and fiber cladding, respectively, were used in the model. In addition, the RIM profile could be treated as invariants along fiber axis for mode calculation, as reported by Nemanja *et al.* [2]. The averaged refractive index n_{ave} of a grating pitch in PbP FBG could be approximated as

$$n_{ave} = \frac{w_v \cdot n_v + (\Lambda - w_v) \cdot n_{co}}{\Lambda} \tag{1}$$

where n_{co} is the refractive index of the fiber core, n_v is the refractive index of the microvoid (i.e., $n_v = 1.0$), w_v is the width of the microvoid and Λ is the grating pitch. The birefringence is given by $\Delta n_B = n_{TE}$ - n_{TM}, where n_{TE} and n_{TM} are the effective indices of the two orthogonal linear polarization states (i.e., TE and TM). To study the effect of area and ellipticity in the cross-sectional pattern of a microvoid on the birefringence, a scan of area A_v was conducted with a constant ellipticity. Then, we repeated the previous process with different ellipticity. The simulation results of birefringence effects from RIMs can be obtained. The mode field profiles and the effective indices of TE and TM modes at the Bragg wavelength of 1547.70 nm were numerically calculated. Fig. 3(a) shows the energy flux profiles of TE and TM modes propagating in a PbP FBG formed by a series of microvoids with an area of 0.60 μm^2 and an ellipticity of 2.51. The calculated birefringence ($\Delta n_B = 7.4815 \times 10^{-5}$) agrees well with the measurement result of FBG S1 (i.e., 7.57×10^{-5}) with an ellipticity of 2.51. Additionally, Fig. 5(b) shows the energy flux profiles of TE and TM modes propagating in the FBG formed by a series of microvoids with the same area of 0.60 μm^2 but a minimized ellipticity of 0.07. Calculation results exhibit that the birefringence is extremely low (i.e., $\Delta n_B = 2 \times 10^{-9}$).

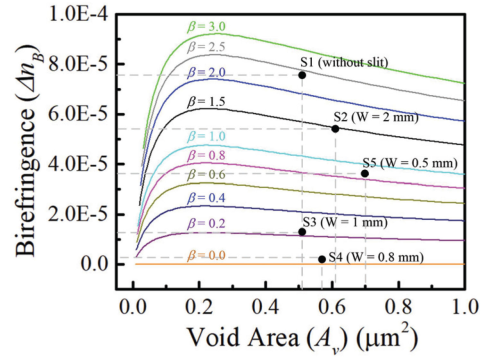

Fig. 4. Calculated birefringence Δn_B as functions of microvoid areas A_v with varying ellipticity β. Black dots show the measured birefringence in five fabricated PbP FBGs (i.e., S1-S5) with different ellipticity β.

TABLE II
PARAMETER COMPARISON OF THREE FBGS (S6-S8)

FBG	*W*/ *mm*	*E*/ *nJ*	*h*/ μm	*w*/ μm	*A*/ μm^2	T_B/ dB	T_{II}/ dB	κ/α
S6	0.4	40.0	1.79	2.87	4.03	-25.67	0.44	58.36
S7	0.3	44.2	1.75	4.35	5.98	-32.01	0.46	69.59
S8	0.2	59.7	1.75	6.30	8.65	-46.65	0.27	172.46

Fig. 4 shows the calculation results of the birefringence Δn_B at the Bragg wavelength of 1547.70 nm as functions of the microvoid area A_v with a series of ellipticities. Obviously, the birefringence Δn_B decreases in case the ellipticity β is reduced, and the birefringence disappears ($\Delta n_B = 0$) when the ellipticity β equals to 0.00 (i.e., the cross-sectional pattern of the microvoid has a complete circular symmetry). Additionally, the microvoid area A_v can also affect the birefringence Δn_B in the PbP FBG. Nevertheless, the influence of A_v is relatively small when A_v is large enough (for example, $A_v = 0.60$ μm^2 for a typical PbP FBG). The measured birefringence Δn_B in FBGs S1-S5, are also displayed in Fig. 4(black dots), and the measured results agree well with the calculated results. Therefore, a low birefringent PbP FBG (i.e., S4, $\Delta n_B = 1.86 \times 10^{-6}$) was achieved by reducing the ellipticity to 0.07 in the cross-sectional pattern of the microvoids with the proposed slit beam shaping method.

C. Inscription of FBG With High κ/α

Subsequently, we studied the slit beam shaping method to increase the RIM area. Three second-order PbP FBGs (i.e., S6, S7 and S8) were inscribed by using femtosecond laser PbP technology and slit beam shaping with decreasing slit width (W) shown in Table II. Note that S6-S8 has the same grating pitch of 1.070 μm and the same grating length of 4 mm. The on-target single pulse energy *E* used for fabricating S6-S8 was shown in Table II. All of them are type II gratings. Figs. 5(a1)–(a3) exhibit the cross-sectional microscope images of the three fabricated FBGs S6-S8, respectively. The width *w*, height *h*, and calculated area *A* in S6-S8 are displayed in Table II. Note

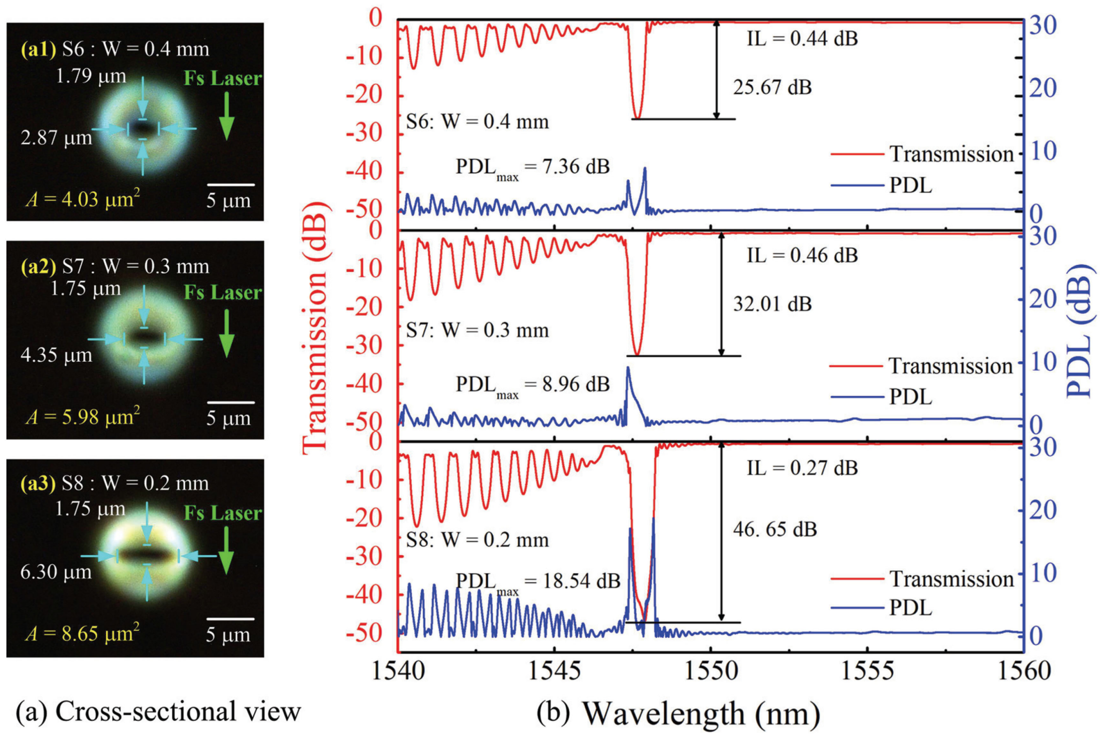

Fig. 5. Three PbP FBGs S6-S8 inscribed by using slit beam shaping with a decreasing slit width W of 0.4, 0.3, and 0.2 mm, respectively. (a) Cross- sectional-view microscope images, and (b) corresponding transmission and reflection spectra of S6-S8.

that an enlarged RIM area can be obtained using a slit with a decreasing slit width. Moreover, Figs. 5(b1)–(b3) show the corresponding transmission and PDL spectra of S6-S8. The measured insertion loss and the dip attenuation S6, S7 and S8 are displayed in Fig. 5(b) and Table II. The ratio of the coupling strength coefficient to the scattering loss coefficient κ/α is a crucial parameter of FBGs, which is identified as a figure of merit for determining the maximum reflectivity achievable with a FBG. The coupling coefficient κ and scattering loss coefficient α can be expressed as

$$\alpha = \frac{\ln(T_{IL})}{-2L}, \tag{2}$$

$$\kappa = \frac{\ln(T_B)}{-2L}, \tag{3}$$

where T_{IL} is the insertion loss (transmission loss measured out-of-band), T_B is the Bragg resonance attenuation, and L is the grating length [13]. It is obvious a higher ratio of κ/α will result in high reflectivity and low insertion loss in the fabricated PbP FBG.

The coupling coefficient κ, scattering loss coefficient α and the ratio of κ/α of the fabricated PbP FBGs of S6, S7 and S8 are calculated and shown in Table II. The maximum ratio of κ/α can be obtained in S8, which is much larger than that (i.e., 70) of the FBG inscribed by use of a conventional femtosecond laser PbP technology [13].

Recently, cylindrical lens-based beam shaping method has also been demonstrated to fabricate a high-quality type II PbP FBG with high reflectivity of 99.99% (i.e., a strong Bragg resonance attenuation of ~47 dB) and a low insertion loss of ~0.80 dB [14]. However, the ratio of κ/α in this PbP FBG was merely 58.75, and hence a long grating length of 10 mm was required to realize such a high-quality type II PbP FBG. These results illustrate that the slit beam shaping will be an effective way to enlarge the RIM area, leading to an increased ratio κ/α in the fabricated PbP FBG. However, FBGs S6-S8 exhibit increasing cladding modes resonance, resulting from the decrease in circular symmetry of RIMs. Additionally, the PDLs in FBGs S6-S8 were measured and displayed in Fig. 5(b). It is obvious that the PDL increases with decreasing slit width due to the increasing ellipticity of the RIMs.

IV. Conclusion

In summary, we demonstrated the fabrication of high-quality FBGs with high reflectivity, low insertion loss, and low birefringence by use of a femtosecond laser PbP technology with a slit beam shaping method. The influence of the slit widths was experimentally studied. The slit beam shaping with an appropriate width could efficiently reduce the ellipticity and create a circular symmetry in the cross-sectional pattern of RIMs, resulting in a decrease in the birefringence. The experimental results agree well with the numerical calculations. Therefore, a high-quality PbP FBG, which has high reflectivity of 99.12% (i.e., Bragg resonance attenuation of 20.52 dB), low insertion loss of 0.30 dB, and low birefringence of 1.86×10^{-6}, was successfully created by using a slit width of 0.8 mm. Moreover, an enlarged cross-sectional area could be inscribed by use of a slit width of 0.2 mm, resulting in a high ratio of 172.46 of the coupling strength coefficient to the scattering loss coefficient in the fabricated PbP FBG, which has very high reflectivity of

99.99% (i.e., a strong Bragg resonance attenuation of 46.65 dB) and low insertion loss of 0.27 dB. Such high-quality FBGs could further be developed for many applications in optical fiber communications, sensors, and lasers.

REFERENCES

[1] X. Y. Liu *et al.*, "Low short-wavelength loss fiber Bragg gratings inscribed in a small-core fiber by femtosecond laser point-by-point technology," *Opt. Lett.*, vol. 44, no. 21, pp. 5121–5124, 2019.

[2] N. Jovanovic *et al.*, "Polarization-dependent effects in point-by-point fiber Bragg gratings enable simple, linearly polarized fiber lasers," *Opt. Exp.*, vol. 17, no. 8, pp. 6082–6095, 2009.

[3] Y. H. Zhu, E. Simova, P. Berini, and C. P. Grover, "A comparison of wavelength dependent polarization dependent loss measurements in fiber gratings," *J. Lightw. Technol.*, vol. 49, no. 6, pp. 1231–1239, Dec. 2000.

[4] P. Lu, D. Grobnic, and S. J. Mihailov, "Characterization of the birefringence in fiber Bragg gratings fabricated with an ultrafast-infrared laser," *J. Lightw. Technol.*, vol. 25, no. 3, pp. 779–786, Mar. 2007.

[5] J. He *et al.*, "Negative-index gratings formed by femtosecond laser overexposure and thermal regeneration," *Sci. Rep.*, vol. 6, 2016, Art. no. 23379.

[6] K. Zhou, M. Dubov, C. B. Mou, L. Zhang, V. K. Mezentsev, and I. Bennion, "Line-by-line fiber Bragg grating made by femtosecond laser," *IEEE Photon. Technol. Lett.,* vol. 22, no. 16, pp. 1190–1192, Aug. 2010.

[7] K. Chah, D. Kinet, M. Wuilpart, P. Mégret, and C. Caucheteur, "Femtosecond-laser-induced highly birefringent Bragg gratings in standard optical fiber," *Opt. Lett.*, vol. 38, no. 4, pp. 594–596, 2013.

[8] X. Z. Xu *et al.*, "Sapphire fiber Bragg gratings inscribed with a femtosecond laser line-by-line scanning technique," *Opt. Lett.*, vol. 43, no. 19, pp. 4562–4565, 2018.

[9] Y. Lai, K. Zhou, K. Sugden, and I. Bennion, "Point-by-point inscription of first-order fiber Bragg grating for C-band applications," *Opt. Exp.*, vol. 15, no. 26, pp. 18318–18325, 2007.

[10] Y. J. Yu, J. D. Shi, F. Han, W. J. Sun, and X. Feng, "High-precision fiber Bragg gratings inscription by infrared femtosecond laser direct-writing method assisted with image recognition," *Opt. Exp.*, vol. 28, no. 6, pp. 8937–8948, 2020.

[11] A. Wolf, A. Dostovalov, K. Bronnikov, and S. Babin, "Arrays of fiber bragg gratings selectively inscribed in different cores of 7-core spun optical fiber by IR femtosecond laser pulses," *Opt. Exp.*, vol. 27, no. 10, pp. 13978–13990, 2019.

[12] Y. P. Wang *et al.*, "Parallel-integrated fiber Bragg gratings inscribed by femtosecond laser point-by-point technology," *J. Lightw. Technol.*, vol. 35, no. 10, pp. 2185–2193, May 2019.

[13] R. J. Williams, N. Jovanovic, G. D. Marshall, G. N. Smith, M. J. Steel, and M. J. Withford, "Optimizing the net reflectivity of point-by-point fiber Bragg gratings: The role of scattering loss," *Opt. Exp.,* vol. 20, no. 12, pp. 13451–13456, 2012.

[14] P. Lu *et al.*, "Plane-by-plane inscription of grating structures in optical fibers," *J. Lightw. Technol.,* vol. 36, no. 4, pp. 926–931, Feb. 2018.

[15] P. S. Salter, M. J. Woolley, S. M. Morris, M. J. Booth, and J. A. J. Fells, "Femtosecond fiber Bragg grating fabrication with adaptive optics aberration compensation," *Opt. Lett.*, vol. 37, no. 24, pp. 5993–5996, 2012.

[16] P. Roldán-Varona, D. Pallarés-Aldeiturriaga, L. Rodríguez-Cobo, and J. M. López-Higuera, "Slit beam shaping technique for femtosecond laser inscription of enhanced plane-by-plane FBGs," *J. Lightw. Technol.,* vol. 38, no. 16, pp. 4526–4532, Aug. 2020.

[17] G. Cerullo *et al.*, "Femtosecond micromachining of symmetric waveguides at 1.5 μm by astigmatic beam focusing," *Opt. Lett.*, vol. 27, no. 21, pp. 1938–1940, 2002.

[18] P. S. Salter *et al.*, "Adaptive slit beam shaping for direct laser written waveguides," *Opt. Lett.,* vol. 37, no. 4, pp. 470–472, 2012.

[19] G. D. Zhang, G. H. Cheng, M. K. Bhyuan, C. D'Amico, Y. S. Wang, and R. Stoian, "Ultrashort bessel beam photoinscription of Bragg grating waveguides and their application as temperature sensors," *Photon. Res.*, vol. 7, no. 7, pp. 806–814, 2019.

[20] M. Ams, G. D. Marshall, D. J. Spence, and M. J. Withford, "Slit beam shaping method for femtosecond laser direct-write fabrication of symmetric waveguides in bulk glasses," *Opt. Exp.*, vol. 13, no. 15, pp. 5676–5681, 2005.

[21] S. Juodkazisa and H. Misawab, "Laser-induced microexplosion confined in a bulk of silica: Formation of nanovoids," *Appl. Phys. Lett.*, vol. 88, 2006, Art. no. 201909.

Xizhen Xu was born in Guangdong, China, in 1990. He received the B.S. degree from the College of Science, Zhejiang University of Technology, Hangzhou, China, in 2013, and the M.S. and Ph.D. degrees in optical engineering from Shenzhen University, Shenzhen, China, in 2016 and 2019, respectively. He is currently with Shenzhen University, Shenzhen, China, as a Postdoctoral Research Fellow. He has authored or coauthored three patent applications and more than 20 journal and conference papers. His current research interests include femtosecond laser micromachining, optical fiber sensors, and fiber Bragg gratings.

Jun He (Member, IEEE) was born in Hubei, China, in 1985. He received the B.Eng. degree in electronic science and technology from Wuhan University, Wuhan, China, in 2006, and the Ph.D. degree in electrical engineering from the Institute of Semiconductors, Chinese Academy of Sciences, Beijing, China, in 2011. From 2011 to 2013, he was with Huawei Technologies, Shenzhen, China, as a Research Engineer. From 2013 to 2015, he was with Shenzhen University, Shenzhen, China, as a Postdoctoral Research Fellow. From 2015 to 2016, he was with The University of New South Wales, Sydney, NSW, Australia, as a Visiting Fellow. Since 2017, he has been with Shenzhen University, Shenzhen, China, as an Assistant Professor or Associate Professor. He has authored or coauthored four patent applications and more than 80 journal and conference papers. His current research interests include optical fiber sensors, fiber Bragg gratings, and fiber lasers. He is a Member of the Optical Society of America.

Jia He was born in Hunan, China, in 1997. She received the B.Eng. degree from the College of Physics and Optoelectronic Engineering, Xiangtan University, Xiangtan, China, in 2019. She is currently working toward the M.S. degree in optical engineering with Shenzhen University, Shenzhen, China. Her current research interests include optical fiber sensors and fiber Bragg gratings.

Baijie Xu was born in Guangdong, China, in 1996. He received the B.Eng. degree in 2019, in optoelectronic information science and engineering from Shenzhen University, Shenzhen, China, where he is currently working toward the master's degree in optical engineering. His main research interests include optical fiber sensing and femtosecond laser processing.

Runxiao Chen was born in Guangdong, China, in 1998. He received the B.Eng. degree from the College of Physics and Optoelectronic Engineering, Shenzhen University, Shenzhen, China, in 2016. He is currently working toward the M.S. degree with Shenzhen University. His current research interests include fiber Bragg gratings and optical fiber sensors.

Kaiming Yang received the B.S. degree in optical information science and technology from East China JiaoTong University, Nanchang, China, in 2012, and the Ph.D. degree from Shenzhen University, Shenzhen, China, in 2019. He is currently with Shenzhen University, Shenzhen, China, as a Postdoctoral Research Fellow. His current research interests include fiber Bragg gratings and femtosecond laser micromachining.

Changrui Liao was born in Shandong, China, in 1984. He is currently with Shenzhen University, Shenzhen, China, as an Associate Professor. His current research interests include femtosecond laser micromachining, optical fiber sensors, and opto-microfluidics.

Yatao Yang received the B.Sc. degree in optical instrumentation engineering from Zhejiang University, Hangzhou, China, and the Ph.D. degree in fiber optics from Glasgow Caledonia University, Glasgow, U.K. After B.Sc., he joined the Institute of Optics and Electronics, Chinese Academy of Sciences, Beijing, China, where he was involved in semiconductor equipment and optoelectronic device development. In 1996, he was with the University of Leeds, Leeds, U.K., as a Research Officer involved in areas of optical fiber laser materials. In 1997, he joined Resonance Ltd., Barrie, ON, Canada, where he was developing spectral gas sensors. In 1998, he joined JDSU Corporation, Canada, where he was developing optical fiber devices. In 2000, he joined Chorum Technologies Inc., Richardson, TX, USA, where he was developing optical fiber devices. In 2004, he joined JDSU Corporation, USA, where he was developing optical fiber devices and fiber lasers. In 2009, he joined NeoPhotonics Corporation, as VP of R&D, developing optical fiber devices. In 2014, he founded Shenzhen Dade Laser Technology Company, Ltd. In 2017, he was appointed as a Distinguished Professor with the College of Information Engineering, Shenzhen University, Shenzhen, China. In 2018, he became the Head of the Smart IoT Center, Shenzhen University. His research interests include optical networking, optical sensors, optical data transmission and data processing, optical nanomaterials, optical-wireless communications, and lasers.

Yiping Wang (Senior Member, IEEE) was born in Chongqing, China, in 1971. He received the B.Eng. degree in precision instrument engineering from the Xi'an Institute of Technology, Xi'an, China, in 1995, and the M.S. and Ph.D. degrees in optical engineering from Chongqing University, Chongqing, China, in 2000 and 2003, respectively. From 2003 to 2005, he was with Shanghai Jiao Tong University, Shanghai, China, as a Postdoctoral Fellow. From 2005 to 2007, he was with Hong Kong Polytechnic University, Hong Kong, as a Postdoctoral Fellow. From 2007 to 2009, he was with the Institute of Photonic Technology, Jena, Germany, as a Humboldt Research Fellow. From 2009 to 2011, he was with the Optoelectronics Research Centre, University of Southampton, Southampton, U.K., as a Marie Curie Fellow. Since 2012, he has been with Shenzhen University, Shenzhen, China, as a Distinguished Professor. He has authored or coauthored one book, 21 patent applications, and more than 240 journal and conference papers. His current research interests include optical fiber sensors, fiber gratings, and photonic crystal fibers. He is a Senior Member of the Optical Society of America and Chinese Optical Society.